

Correlation of Outer Nuclear Layer Thickness With Cone Density Values in Patients With Retinitis Pigmentosa and Healthy Subjects

Moreno Menghini,¹ Brandon J. Lujan,^{2,3} Shiri Zayit-Soudry,¹ Reema Syed,¹ Travis C. Porco,^{1,4,5} Kristine Bayabo,² Joseph Carroll,⁶⁻⁸ Austin Roorda,² and Jacque L. Duncan¹

¹Department of Ophthalmology, University of California, San Francisco, San Francisco, California, United States

²School of Optometry and Vision Science Graduate Group, University of California, Berkeley, Berkeley, California, United States

³West Coast Retina Medical Group, San Francisco, California, United States

⁴Department of Epidemiology and Biostatistics, University of California, San Francisco, San Francisco, California, United States

⁵El. Proctor Foundation for Research in Ophthalmology, University of California, San Francisco, San Francisco, California, United States

⁶Department of Ophthalmology, Medical College of Wisconsin, Milwaukee, Wisconsin, United States

⁷Department of Cell Biology, Neurobiology & Anatomy, Medical College of Wisconsin, Milwaukee, Wisconsin, United States

⁸Department of Biomedical Engineering, Marquette University, Milwaukee, Wisconsin, United States

Correspondence: Jacque L. Duncan, UCSF Department of Ophthalmology, 10 Koret Way, K129, San Francisco, CA 94143-0730, USA; duncanj@vision.ucsf.edu.

Submitted: August 21, 2014
Accepted: November 25, 2014

Citation: Menghini M, Lujan BJ, Zayit-Soudry S, et al. Correlation of outer nuclear layer thickness with cone density values in patients with retinitis pigmentosa and healthy subjects. *Invest Ophthalmol Vis Sci.* 2015;56:372-381. DOI:10.1167/iovs.14-15521

PURPOSE. We studied the correlation between outer nuclear layer (ONL) thickness and cone density in normal eyes and eyes with retinitis pigmentosa (RP).

METHODS. Spectral-domain optical coherence tomography (SD-OCT) scans were acquired using a displaced pupil entry position of the scanning beam to distinguish Henle's fiber layer from the ONL in 20 normal eyes (10 subjects) and 12 eyes with RP (7 patients). Cone photoreceptors were imaged using adaptive optics scanning laser ophthalmoscopy. The ONL thickness and cone density were measured at 0.5° intervals along the horizontal meridian through the fovea nasally and temporally. The ONL thickness and cone density were correlated using Spearman's rank correlation coefficient r .

RESULTS. Cone densities averaged over the central 6° were lower in eyes with RP than normal, but showed high variability in both groups. The ONL thickness and cone density were significantly correlated when all retinal eccentricities were combined ($r = 0.74$); the correlation for regions within 0.5° to 1.5° eccentricity was stronger ($r = 0.67$) than between 1.5° and 3.0° eccentricity ($r = 0.23$). Although cone densities were lower between 0.5° and 1.5° in eyes with RP, ONL thickness measures at identical retinal locations were similar in the two groups ($P = 0.31$), and interindividual variation was high for ONL and cone density measures. Although ONL thickness and retinal eccentricity were important predictors of cone density, eccentricity was over 3 times more important.

CONCLUSIONS. The ONL thickness and cone density were correlated in normal eyes and eyes with RP, but both were strongly correlated with retinal eccentricity, precluding estimation of cone density from ONL thickness. (ClinicalTrials.gov number, NCT00254605.)

Keywords: outer nuclear layer thickness, cone density, optical coherence tomography, adaptive optics scanning laser ophthalmoscopy, retinitis pigmentosa

Outer nuclear layer thickness (ONL) measured using spectral-domain optical coherence tomography (SD-OCT) has been used to provide an indirect, noninvasive measure of photoreceptor survival when studying photoreceptor degeneration in human eyes and mouse models of retinal degeneration.¹⁻⁴ The normal ONL contains rod and cone photoreceptor nuclei throughout the retina with the exception of a rod-free zone approximately 350 μm in diameter, extending 100 to 200 μm from the foveal center, in which only cones are present; rods and cones are present in equal density at 400 to 500 μm from the foveal center, and rod nuclei predominate the ONL at locations eccentric to 500 μm .⁵

Noninvasive studies in which SD-OCT measures of retinal thickness are compared to en face images of cone photorecep-

tors in human subjects have not shown consistent correlations between ONL thickness and cone density values, perhaps because rod and cone photoreceptor nuclei contribute to ONL thickness, while cone photoreceptors are most readily imaged noninvasively using en face, adaptive optics (AO) techniques.⁶ Curcio et al.^{7,8} compared OCT with histological data in eyes without retinal degeneration and found that parafoveal ONL thickness increases and the Henle's fiber layer (HFL) thickness may increase with age, although rod photoreceptor numbers decrease with age. Chui et al.⁶ measured cone density using AO scanning laser ophthalmoscopy (AOSLO) and found ONL thickness increased, while cone density decreased, with age. These results could reflect changes associated with age-related

remodeling of retinal structures within the boundaries used for ONL measurements with OCT.

Lujan et al.⁹ developed a technique called directional OCT (D-OCT), in which images are acquired with a displaced pupil entry position, resulting in a reflectivity change that provides the optical contrast necessary to distinguish the HFL from the true ONL. The current study used D-OCT to distinguish the ONL from the HFL, and compared “true” ONL thickness with cone density values at identical retinal locations in normal eyes and patients with retinitis pigmentosa (RP).

MATERIALS AND METHODS

In this cross-sectional study, D-OCT and AOSLO images were acquired during a single session as part of a prospective clinical trial (NCT00254605) using high-resolution retinal imaging to characterize photoreceptor structure in normal subjects and patients with RP. All subjects provided written informed consent. This study was approved by the Institutional Review Boards of the University of California, San Francisco and the University of California, Berkeley, and adhered to the tenets of the Declaration of Helsinki.

Clinical Examination

A complete history was obtained, including information about all known family members. Best-corrected visual acuity (VA) and refractive error were measured according to the Early Treatment of Diabetic Retinopathy Study protocol, Goldmann kinetic perimetry was measured in a light-adapted state using V4e and I4e targets, and total visual field area seen was calculated by adding seeing areas and subtracting scotomatous areas along every meridian. Axial length was measured noninvasively using partial coherent interferometry with short-coherence infrared light (780 nm wavelength; Carl Zeiss Meditec, Inc., Dublin, CA, USA), as described previously.^{10,11} Whole blood was obtained for mutation analysis in four of seven patients who had forms of RP for which genetic testing was available; two patients were tested through the eyeGENE consortium (National Eye Institute, National Institutes of Health [NIH], Bethesda, MD, USA) for molecular analysis of genes associated with x-linked RP (patient 40015) or with autosomal dominant RP (patient 10048); no disease-causing mutations were identified in 10048. Genetic testing for mutations associated with Ashkenazi heritage for patient 40030 was performed through the Carver nonprofit genetic testing laboratory (Iowa City, IA, USA); no disease-causing mutations were identified in the *DHDDS*, *LCA5*, *MAK*, *PCDH15*, or *USH3A* genes. Genetic testing was performed through a research protocol (Radha Ayyagari, PhD, Project #081869, University of California, San Diego, San Diego, CA, USA) using whole exome sequencing in families with autosomal recessive RP from a consanguineous pedigree (patient 40032). Genetic testing was not performed on isolated RP cases without a history of Ashkenazi Jewish descent or a family history of consanguinity (patients 30015, 40058, and 40060).

D-OCT Data Collection and HFL Thickness Measurements

The SD-OCT (Spectralis HRA+OCT; Heidelberg Engineering, Heidelberg, Germany) scans were obtained using standard and displaced pupil entry positions. The D-OCT image protocol included a horizontal scan through the fovea using a central scanning laser entry position, and two additional horizontal scans acquired using nasally- and temporally-displaced pupil

entry positions, as previously described (Fig. 1).⁹ Varying the pupil entry position causes an apparent tilt to the horizontal B-scan due to differing optical path-lengths.⁹ The automated real time (ART) fundus-tracking system was used to average 100 scans for each image.

The horizontal B-scans acquired using displaced pupil entry positions were used to identify the HFL and measure the ONL thickness. A second-order polynomial 2-D spatial transformation was performed with Adobe Photoshop (Adobe, Inc., San Jose, CA, USA) to obtain registered sets, which were verified by toggling between images.¹² Total retinal thickness from the internal limiting membrane (ILM) to Bruch’s membrane was measured in each subject, and no change occurred after transformation. Registration was graded as acceptable if motion of either the ILM or RPE contours was undetectable. Images were registered pairwise between the flat image and a single inclined image, and then the flat image and other inclined images to result in a composite stack of three images of the same part of the macula having been acquired through the three different pupil positions. These B-scans were exported to ImageJ (Rasband WS, 119–2012; <http://imagej.nih.gov/ij/>; provided in the public domain by the National Institutes of Health, Bethesda, MD, USA) where the multipoint selection tool was used to mark five different retinal layers: ILM, transition between the outer plexiform layer (OPL) and HFL, transition between the HFL and the ONL, external limiting membrane (ELM), and outer edge of the RPE. For each layer 40 points were selected by a single grader. The ONL thickness was defined as the distance between the inner edge of the ELM to the outer edge of the HFL (Fig. 2). Only scans that allowed complete visualization of the transition between OPL, HFL, and ONL were used for measurements. Central retinal thickness (CRT) was defined as the vertical distance from the inner edge of the ILM to the outer edge of the RPE at the thinnest point within the foveal pit. Layer segmentation data were processed using custom-written software in MatLab (MathWorks, Inc., Natick, MA, USA). To assess OCT segmentation repeatability, the same grader repeated the segmentation at a second time point separated from the first session by 4 weeks to 4 months, independent from and masked to the initial OCT layer selection.

AOSLO Image Acquisition and Cone Structure Analysis

High-resolution image acquisition with AOSLO and postacquisition processing were performed as described previously.^{10,13} For each subject the AOSLO image montage was precisely aligned with the near-infrared (NIR) fundus image acquired simultaneously with the D-OCT image (Adobe Illustrator; Adobe, Inc.), and the scan line on the NIR image was used to align the location of the D-OCT B-scan with the AOSLO montage. Using custom-written software regions of interest (ROIs) were selected on the AOSLO montage located along the line indicating the location of the D-OCT scan. The area imaged at each ROI measured 10 × 10 arcminutes and the ROIs were spaced 0.5° apart. Using these settings, four to six ROIs were selected nasally and temporally along the horizontal scan through the fovea, depending on the quality and size of the AOSLO montage (Fig. 3). Cone spacing measures were performed by two independent graders (Graders 1 and 2) using previously described methods.^{10,13} Cone spacing was chosen because the measures are least affected by image quality and do not require the identification of every single cone within a ROI. Cone spacing measures were converted to cone density values (cones/degree²) assuming hexagonal packing of the cone mosaic. To test this assumption, a subset of patients in which every cone in the mosaic was clearly

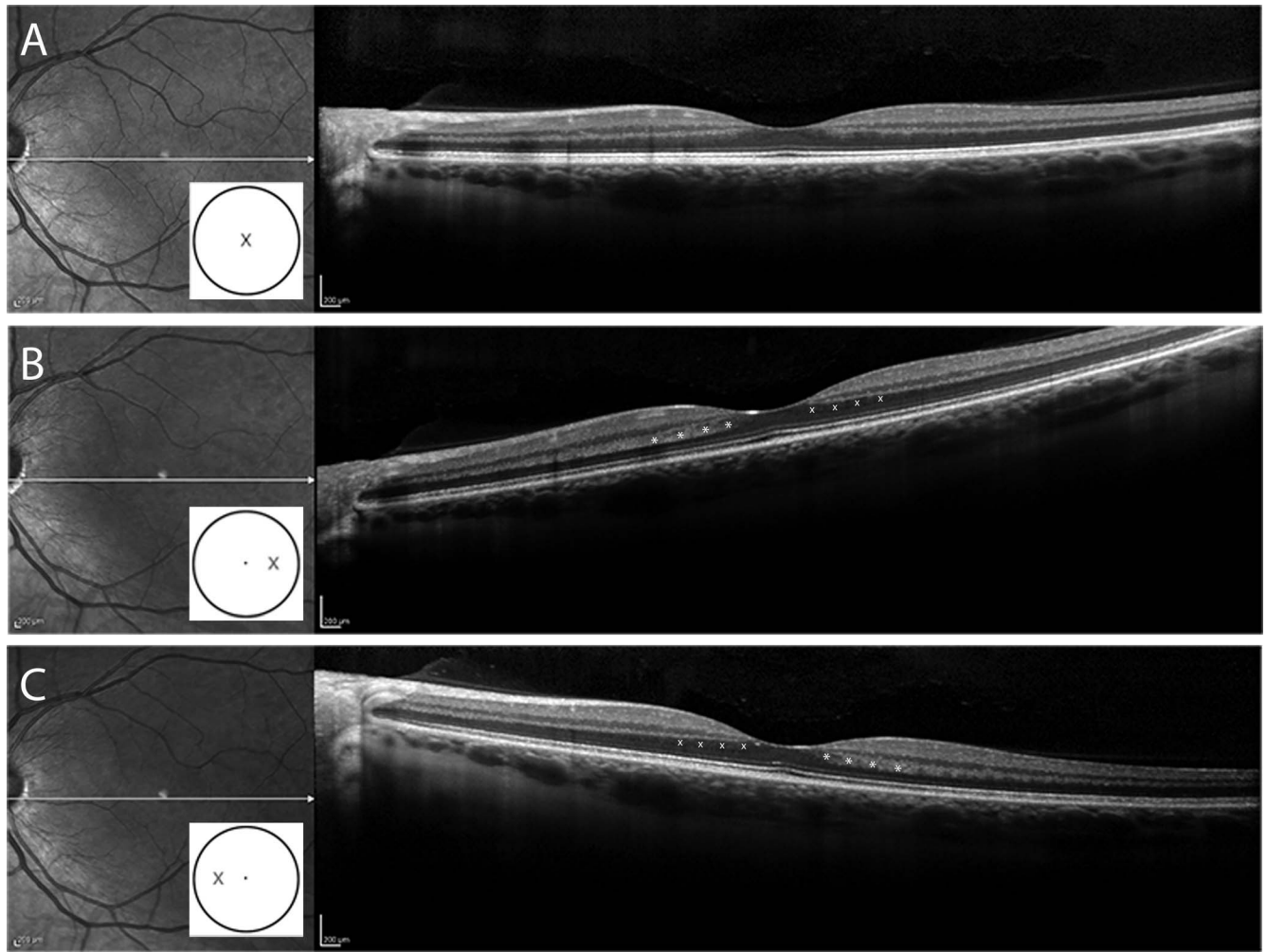


FIGURE 1. The SD-OCT images acquired using conventional and directional (D-OCT) acquisition techniques. (A) Infrared fundus image with a horizontal SD-OCT B-scan through the fovea in a normal subject acquired through the center of the fovea. (B) Horizontal SD-OCT B-scan through the fovea in the same subject using D-OCT in which the incident light enters at the temporal edge of the pupil, while (C) shows D-OCT from the same subject with incident light displaced to the nasal edge of the pupil. With a variation of the incident light the HFL can be revealed as a hyper- (*) or hyporeflective (°) region adjacent to the OPL. The *white cartoon inset* shows the pupil entry position of the scanning laser beam.

visible was used to determine cone density values directly (CD) and compared to cone density values derived from cone spacing measures from each grader. We computed the pairwise difference between CD and Grader 1, CD and Grader 2, and Graders 1 and 2. We compared the mean absolute difference between the first two of these and the third to estimate whether or not CD was more different from Graders 1 and 2 than the difference between the cone density values derived by

Graders 1 and 2. The *P* value was estimated by permutation of the values for CD, Grader 1, and Grader 2 within each subject.

Statistical Analysis

Age was compared between patients and normal subjects using the Wilcoxon rank sum test; axial length, spherical equivalent (SE) and VA were compared using linear mixed

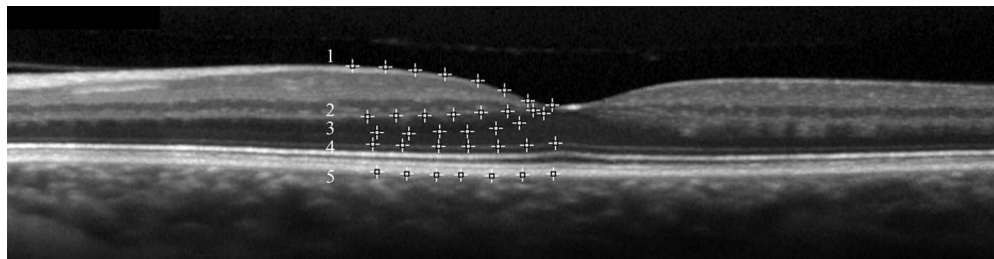


FIGURE 2. The D-OCT image of a normal subject illustrates the method of retinal layer segmentation using the multipoint selection tool of ImageJ. The ONL thickness was defined as the distance between the inner edge of the ELM (4) to the outer edge of the HFL (3). 1, ILM; 2, the transition between the OPL and the HFL; 3, the transition between the HFL and the ONL; 4, ELM; 5, the outer edge of the RPE.

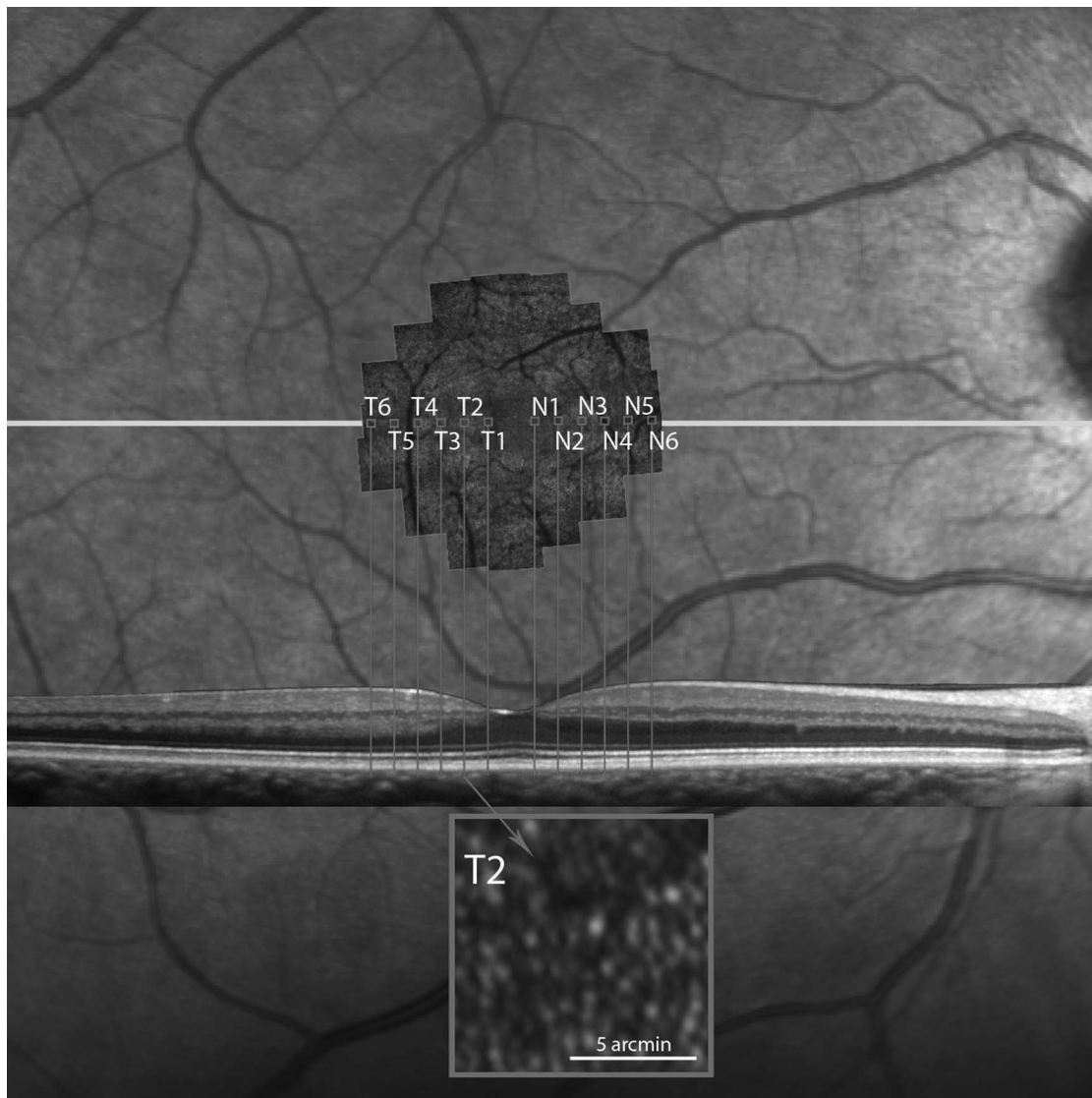


FIGURE 3. The AOSLO montage aligned with the B-scan SD-OCT image and the near-infrared fundus image. The capital letters *N* (nasal) and *T* (temporal) show the selected retinal regions along the central horizontal meridian with the respective locations on the SD-OCT B-scan. The *inset* in *gray* shows a representative cone mosaic at location T2 in this normal eye.

effects regression. Goldmann targets V4e and I4e were compared using the Wilcoxon rank sum test. Comparisons of cone density between two graders were conducted using the consistency intraclass correlation. Average ONL thickness measurements made at each time were used for statistical comparison. Correlation between estimated cone density and ONL thickness at each region was assessed using the Spearman rank correlation r . Differences between Spearman rank correlations between regions within each eye and between patients and normal subjects were assessed using bootstrap resampling by subject (clustered bootstrap), accounting for the correlation between measurements taken on different regions within the same eye, and between the two eyes of the same subject. To determine the relative importance of eccentricity and ONL thickness in explaining cone density, we used the decomposition method as described by Lindeman et al.¹⁴ with approximate 95% bootstrap percentile confidence intervals (CIs) generated by resampling eyes, which yields a normalized importance score for each predictor; the importance scores are between 0 and 1, and sum up to 1. We used ordinary linear

regression to model the cone density, using eccentricity and ONL thickness up to the second order. All calculations were conducted using R v. 3.0 (packages irr and lme4; R Foundation for Statistical Computing, Vienna, Austria).

RESULTS

Study Population

Clinical characteristics of the study participants are summarized in Table 1. We analyzed 20 normal eyes (10 subjects) and 12 eyes (7 patients) with RP. The normal subjects were older (mean 48.3 ± 11 years) than the patients (35.7 ± 11 years), but not significantly ($P = 0.06$, Wilcoxon rank sum test). There were more female patients (58%) than normal subjects (30%). The VA was excellent in both groups, but statistically significantly better in the normal population ($P = 0.002$). The visual field areas (Goldmann targets V4e and I4e) were statistically significantly smaller in the patients ($P = 0.004$ and <0.001 , Wilcoxon rank sum test). The SE of the patients

TABLE 1. Normal Subjects and RP Patients Included in the Study

Study ID	Age	Sex	Eye	Sphere	Cylinder	SE	VA	Axial Length	CRT	V4e Area	I4e Area
Normal subjects											
40053	38	F	OD	-0.50	-0.25	-0.38	1.00	23.74	221	1659	1264
40053	38	F	OS	-0.25	-0.25	-0.13	1.00	24.03	223	1676	1246
40054	24	F	OD	-0.25	0.00	-0.25	1.25	25.11	218	1619	1317
40054	24	F	OS	0.00	-0.25	0.13	1.25	25.36	224	1619	1444
10022	64	M	OD	0.75	-0.25	0.88	1.25	24.1	251	1592	1147
10022	64	M	OS	0.00	-1.00	0.50	1.25	24.15	250	1546	1176
10023	57	M	OD	0.00	1.00	-0.50	2.00	23.5	258	1575	1221
10023	57	M	OS	0.00	-1.25	0.63	1.60	23.26	245	1546	1116
10033	57	M	OD	0.75	-0.50	1.00	1.25	23.96	243	1621	1175
10033	57	M	OS	0.50	0.00	0.50	1.25	24.07	239	1565	1085
30016	44	F	OD	-3.00	0.00	-3.00	1.60	23.91	234	1508	1339
30016	44	F	OS	-2.75	-0.25	-2.63	1.60	23.72	231	1576	1374
40048	51	M	OD	0.00	-0.50	0.25	1.60	23.7	251	1649	1323
40048	51	M	OS	0.00	-0.50	0.25	1.60	23.84	263	1684	1377
40051	48	M	OD	0.50	-0.50	0.75	1.60	23.74	221	1636	1427
40051	48	M	OS	0.25	-0.50	0.50	1.60	23.68	225	1581	1412
40055	50	M	OD	-0.25	0.00	-0.25	1.60	23.93	235	1636	1259
40055	50	M	OS	-0.75	0.00	-0.75	1.25	23.84	241	1590	1278
40061	50	M	OD	0.25	-1.75	1.13	1.25	24.28	258	1506	1227
40061	50	M	OS	0.25	-1.25	0.88	1.25	24.14	258	1499	1262
Mean	48.3					-0.03	1.40	24.00	239	1594.15	1273.45
SD	11.0					1.09	0.25	0.49	15	55.28	103.35
Patients											
30015-RP	41	M	OD	-3.50	-2.00	-2.50	0.63	25.45	251	1217	519
30015-RP	41	M	OS	-3.00	0.50	-3.25	0.50	25.04	248	1168	454
10048-RP	41	F	OD	0.00	-1.25	0.63	1.00	22.93	204	787	124
40030-RP	40	F	OD	-3.25	0.00	-3.25	1.60	23.26	231	1406	1358
40030-RP	40	F	OS	-3.75	0.00	-3.75	1.25	23.46	261	1601	1245
40015-XLRP	49	M	OD	-3.50	-2.00	-2.50	0.63	25.45	216	607	96
40032-ARRP	30	M	OD	0.50	-4.00	2.50	0.80	23.61	192	1651	760
40032-ARRP	30	M	OS	-0.75	-4.25	1.38	0.80	24.17	218	1659	918
40058-RP	25	F	OD	-6.25	-0.75	-5.88	1.00	25.53	278	648	454
40058-RP	25	F	OS	-7.00	-0.75	-6.63	1.00	25.35	278	642	500
40060-RP	63	F	OD	0.25	-1.50	1.00	1.25	23.47	239	1092	302
40060-RP	63	F	OS	-0.25	-0.75	0.13	1.25	23.45	250	1132	346
Mean	35.7					-1.84	0.98	24.26	240	1134.17	589.67
SD	11.0					2.94	0.32	1.02	29	395.57	405.55
<i>P</i>	0.06					<0.001	0.002	0.39	0.62	0.004	<0.001

VA was reported as the quotient (20/20 = 1.0). Age is shown in years. Sphere, cylinder, and SE are shown in diopters. Axial length is in millimeters. CRT is in micrometers. Visual field is reported as total degrees of visual field seen in response to the Goldmann V4e and I4e targets. RP, simplex RP; XLRP, x-linked RP due to homozygous p.Glu809GlyfsX25 mutation in the *RPGR* gene; ARRP, autosomal recessive RP associated with homozygous p.Gly1961Glu mutations in the *ABCA4* gene; M, male; F, female.

was more myopic than the normal subjects ($P < 0.001$, linear mixed model), but the axial lengths were not significantly different between the groups ($P = 0.39$, linear mixed model) (Table 1).

Outcome Measures

The mean (\pm SD) CRT was $239 \pm 15 \mu\text{m}$ in normal eyes and $240 \pm 29 \mu\text{m}$ in eyes with RP ($P = 0.62$, linear mixed model, controlling for sex). Within normal eyes, the mean CRT in female eyes ($224 \pm 6 \mu\text{m}$) was thinner than in male eyes ($245 \pm 13 \mu\text{m}$, $P = 0.009$). In eyes with RP, the mean CRT in female eyes ($253 \pm 22 \mu\text{m}$) was thicker than in male eyes ($217 \pm 30 \mu\text{m}$, $P = 0.15$), likely because more males than females with advanced disease were studied. The ONL thickness at each retinal location was not significantly different between normal subjects and patients ($P = 0.31$, linear mixed model, adjusting for retinal location and sex), and the interindividual variation

for ONL thickness measures at each location was high (SD/mean ONL thickness = 13% to 23% for normal eyes, 1% to 28% for patient eyes (Table 2).

Figure 4 plots the cone densities of the normal and RP retinas as a function of location (see also Table 2). Overall, cone densities were significantly lower in eyes with RP compared to normal eyes. The comparison of each single retinal location separately also revealed lower average cone densities in eyes with RP compared to normal eyes, although it did not reach statistical significance at individual retinal locations (Table 2), and interindividual variation in cone density at each location was high (SD/mean CD = 9%–17% in normal eyes, 17%–33% in patient eyes, Table 2). Although histological studies have demonstrated higher cone densities in nasal compared to temporal retina,⁵ we did not detect a significant differences in average cone densities in the nasal compared to the temporal retina in either patients or normal

TABLE 2. Mean ONL Thicknesses (\pm SD), CD Measures (\pm SD), and Spearman's Rank Correlation Coefficient r for Each Retinal Location for All Normal Subjects and Patients

	Normal Eyes						Patient Eyes					
	<i>n</i>	ONL	SD	CD	SD	<i>r</i>	<i>n</i>	ONL	SD	CD	SD	<i>r</i>
N1	20	82	10	5905	988	-0.12	7	87	1	5009	875	-0.20
N2	20	60	8	4310	619	0.32	11	63	18	3433	1153	0.60
N3	20	46	8	3406	345	0.33	12	44	10	2873	943	0.57
N4	20	40	7	2779	316	0.26	11	36	6	2501	616	0.33
N5	20	38	6	2387	259	0.32	9	36	4	2248	492	-0.61
N6	20	38	6	2049	257	-0.02	8	34	7	1977	409	-1.00
T1	20	73	17	6076	926	-0.38	7	71	19	4554	1655	0.20
T2	20	52	11	4389	509	0.30	9	54	14	3776	1139	0.26
T3	20	44	8	3494	508	0.63	10	41	9	2816	901	0.43
T4	20	40	7	2723	318	0.37	11	37	8	2472	641	0.29
T5	20	39	6	2422	232	0.25	11	34	7	2154	491	0.07
T6	20	38	5	2091	193	0.29	9	30	7	1962	355	0.43

N1 and T1 are 0.5° from the fovea with each subsequent location separated by 0.5°. N, retinal locations nasal to the fovea; T, locations temporal to the fovea.

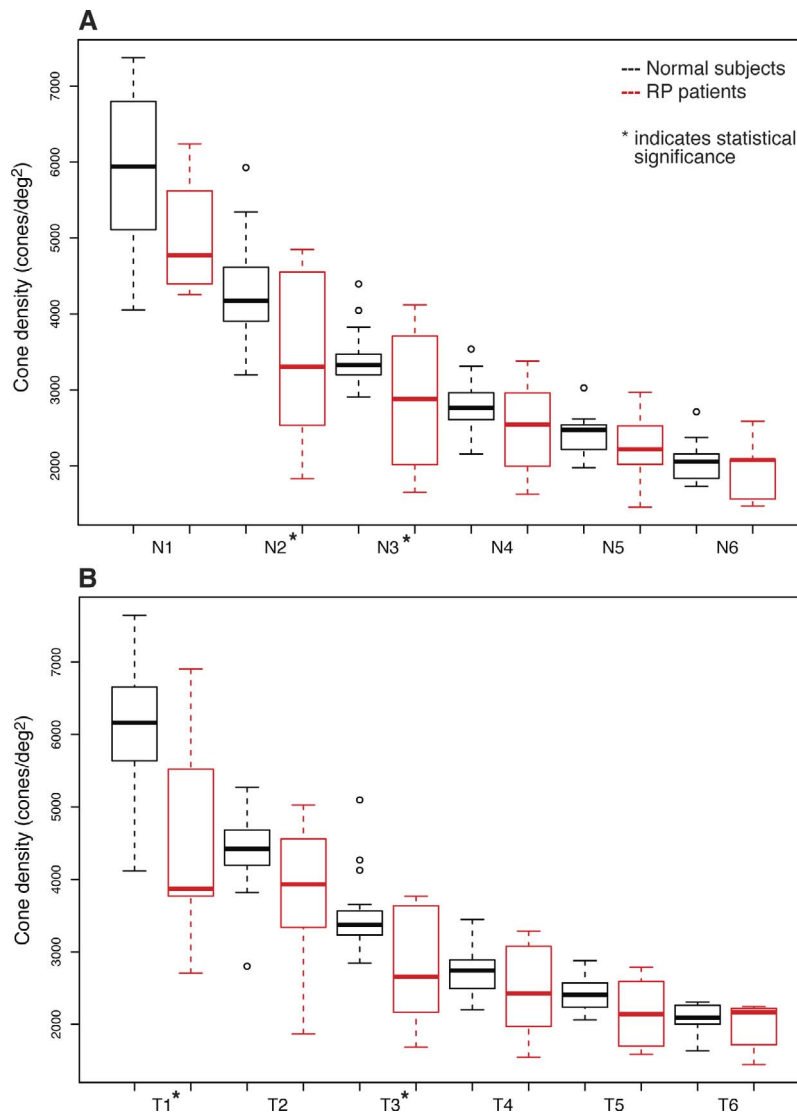


FIGURE 4. Tukey box plot of the average cone densities in normal eyes and eyes with RP at each single retinal location. The *band* inside the *box* is the median. The *bottom* and *top* of the *box* represent the first and third quartile, the *whiskers* are within 1.5 interquartile range (IQR) of the lower and upper quartile. Any data not included between the *whiskers* is an outlier and is plotted with a *small circle*. (A) Shows nasal retinal locations, and (B) temporal retinal locations.

TABLE 3. The CD (Cones/deg²) Measured From a Subset of Images Where the Identification of Every Single Cone was Possible Within One ROI

Subject	Eye	ROI	CD	Grader 1	Grader 2
40058	OS	N3-4	3712	3802	3695
40058	OD	T5-6	2256	2473	2307
40060	OS	N2	3392	3522	3501
40060	OD	N5	1936	1948	1835
30015	OS	T3	3488	3829	3868
30015	OD	T5	2448	2147	1999

Columns 5 (Grader 1) and 6 (Grader 2) show the cone density values converted from cone spacing measures, assuming a hexagonal pattern at similar retinal eccentricity. Column 3 shows the retinal location, where N stands for nasal and T for temporal. N2 is located at 1.0° nasal to the fovea, and subsequent ROIs are separated by 0.5° spacing intervals as described in the Materials and Methods.

subjects ($P = 0.96$ and 0.69 , respectively, linear mixed model, clustering for eye and patient). To evaluate the decision to convert cone spacing to cone density assuming a hexagonal packing pattern, cone density was measured directly in a subset of patient eyes in which at least one ROI enabled identification of every single cone in the mosaic ($n = 6$); values were comparable to the cone density values computed from the cone spacing ($P = 0.09$, permutation test, Table 3).

Both ONL thickness and cone densities decreased with increasing eccentricity from the fovea (Table 2). A statistically significant positive correlation was found between cone density and the overlying ONL thickness when considering all eccentricities (Spearman correlation, $r = 0.74$; 95% CI, 0.67–0.82; clustered bootstrap; Fig. 5A), with similar results in normal eyes ($r = 0.74$; 95% CI, 0.67–0.82; Fig. 5B) and eyes with RP ($r = 0.70$; 95% CI, 0.48–0.88; Fig. 5C). The ONL

thickness and cone density between 0.5° and 1.5° eccentricity were more strongly correlated ($r = 0.67$; 95% CI, 0.55–0.81; Fig. 5D), than regions from 1.5° to 3.0° ($r = 0.23$; 95% CI, –0.06 to 0.48; Fig. 5E); the difference between these regions was statistically significant (95% CI, 0.27–0.63). The correlation was highly variable for normal subjects and RP patients when individual locations were analyzed (Table 2). The relationship between retinal eccentricity, ONL thickness, and cone density then was evaluated. The normalized relative importance of eccentricity was 0.77 (0.65–0.85), and of thickness was 0.22 (0.14–0.32, the relative importance of the interaction term was 0.013 [0.005–0.041]). We found that eccentricity and ONL thickness were important predictors of cone density, though eccentricity was over 3 times as important as ONL thickness. The Spearman correlation analyses did not differ significantly when computed with ONL+HFL thickness instead of ONL thickness measured using D-OCT (data not shown).

Modeling the relationship between ONL thickness and cone density as a function of degrees from the foveal center revealed a regression coefficient of 37.2 (95% CI, 30.1–44.2) cones/deg² per μm retinal thickness, including all eyes and all regions for normal subjects and RP patients. When normal and RP eyes were compared separately, the regression coefficients were 35.6 (95% CI, 27.7–43.5) and 32.8 (95% CI, 21.8–43.8), respectively ($P = 0.82$, controlling for degree and subject and interaction). The intergrader variability for the cone density and the intragrade variability for the ONL thickness showed good agreement, with ICC = 0.95 (95% CI, 0.93–0.96) and ICC = 0.91 (95% CI, 0.88–0.92), respectively.

DISCUSSION

The present study compared measures of cone photoreceptor structure by measuring the ONL thickness using D-OCT to

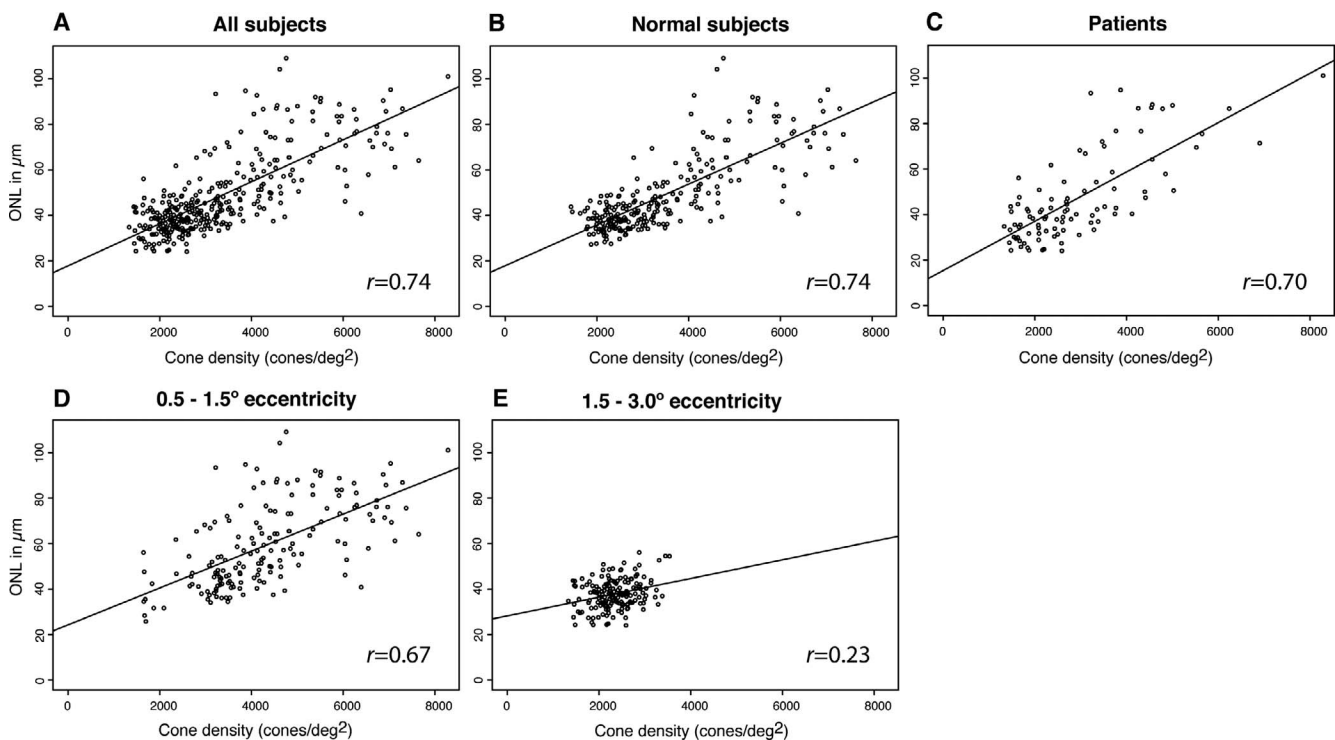


FIGURE 5. Correlation between cone density and ONL thickness for all subjects (A), Spearman's rank correlation coefficient [r] = 0.74; 95% CI, 0.67–0.82), normal subjects (B), $r = 0.74$; 95% CI, 0.67–0.82), patients (C), $r = 0.70$; 95% CI, 0.48–0.88) as well as for regions between 0.5° and 1.5° eccentricity (D), $r = 0.67$; 95% CI, 0.55–0.81), and regions between 1.5° and 3° eccentricity (E), $r = 0.23$; 95% CI, –0.06–0.48), only.

isolate the ONL from the HFL components of cross-sectional SD-OCT images and cone photoreceptor spacing using AOSLO en face images. The ONL thickness and cone density were correlated in normal subjects and patients with RP. The relationship between ONL thickness and cone density was strongest at locations between 0.5° and 1.5° eccentricity, where cones likely predominate the ONL thickness, and decreased at more eccentric (1.5° – 3.0°) regions. However, the interindividual variability (as manifest by standard deviation values) of ONL thickness and cone density at single retinal locations was high (Table 2; Fig. 4), in accordance with published data.^{5,15,16} The high variability also is reflected in the wide range of values around the best fit regression line (Fig. 5) and the range of correlation coefficients when retinal locations were analyzed individually (Table 2). Eccentricity and ONL thickness were important predictors of cone density, but eccentricity was over 3 times as important as ONL thickness. The correlation between ONL thickness and cone density is not strong enough to reliably predict cone density from ONL thickness at any given retinal location, and is likely due largely to the relationship between retinal eccentricity, and cone density and ONL thickness.

The resolution limits of the AOSLO system used in this study did not permit acquisition of rod photoreceptors which, depending on the distance to the fovea, significantly contribute to ONL thickness. According to histological data, rods and cones are present at equal densities beginning at approximately 400 to 500 μm from the foveal center,⁵ which corresponds to an eccentricity of approximately 1.5° (300 $\mu\text{m}/\text{deg}$). Regions from 0.5° to 1.5° eccentricity showed a stronger correlation between ONL thickness and cone density than regions from 1.5° to 3.0° , which showed no significant correlation. The lower correlation found in the current study for eccentricities greater than 1.5° may reflect the increasing number of rod photoreceptors contributing to the ONL thickness in regions at these locations. However, we would expect higher correlations at the retinal regions closest to the fovea (regions N1 and T1 at 0.5° eccentricity); correlation coefficients at single retinal locations were highly variable and did not reveal a pattern with better correlations in rod-free or presumed low rod-count regions (Table 2). Due to the resolution limits of our AOSLO system we could not obtain quantifiable images of foveal cones in all subjects; perhaps correlating ONL thickness at the fovea with foveal cone spacing measures would demonstrate a closer correlation between OCT measures of ONL thickness and cone spacing measures using AOSLO. Finally, the significant correlation values obtained for the binned regions, including locations between 0.5° and 1.5° , were substantially eccentricity-driven. Taken together, the findings indicated that ONL thickness, even when the HFL is excluded with D-OCT, cannot be used to predict cone density accurately.

Previous studies comparing the ONL thickness (including HFL) with cone density using AOSLO found that average cone densities were lower, but ONL+HFL thicknesses were greater, in older subjects.⁶ A comparison of histological sections studied with SD-OCT showed that the ONL is much thinner in histological sections compared to SD-OCT images, due not only to the overall thinner histological sections (nonlinear tissue shrinkage due to dehydration and sectioning stress), but more importantly to the HFL, since the ONL band in SD-OCT contains the histologic ONL and HFL.⁷ In contrast, the OPL band in SD-OCT is thinner than the histologic OPL, because it does not include the HFL. The inner aspect of the ONL as visualized by SD-OCT inconsistently contains the HFL.^{7,17–19} To overcome a possible contribution of the HFL to the ONL thickness, we distinguished the HFL from ONL thickness measurements by obtaining D-OCT images.⁹ The measurement of true ONL thickness without contribution from HFL did not

reveal a more consistent relationship between ONL thickness and cone density in the present study. Thus, our results are similar to other reports which included HFL in their measurements.⁶

The *in vivo* measurement of cone photoreceptors with AOSLO has been used to assess cone structure in normal subjects and patients with retinal degenerations.^{10,13,20–23} The reproducibility of AOSLO measures in the present study, as graded by two experienced independent readers, was high. Cone density was calculated from cone spacing assuming a hexagonal packing of the cone mosaic. In eyes with RP, hexagonal packing of the mosaic may be lost during disease progression, and such an assumption would be erroneous. Cone density was measured directly in a subset of patients with RP, where at least one ROI enabled identification of every cone in the mosaic (Table 3). Comparison of the directly measured cone density values with the numbers calculated from cone spacing did not reveal a statistically significant difference in this study ($P = 0.09$, Table 3).

Cone density was lower in patients compared to normal subjects, but ONL thickness was similar in both groups. In the current study, the patients had a higher average myopic refractive error, but the axial lengths were not significantly different between normal eyes and eyes with RP. According to Li et al.²⁴ we would not expect differences in the cone spacing with comparable axial lengths despite differences in refractive error.

In RP, photoreceptor outer segments are lost earliest, followed by loss of inner segments, and finally loss of the photoreceptor nuclei.^{25,26} Since the ONL comprises cone and rod nuclei, the discrepancy between ONL thickness and cone density may be due to the contribution of rod nuclei in the ONL, since rods were not visualized or quantified in the current study. However, in RP rods degenerate earlier than cones, so the observation that the ONL thickness remains normal in the context of reduced cone density at a number of locations in the RP patients may suggest that the ONL thickness is not as sensitive to early photoreceptor degeneration as AOSLO measures of cone density. Secondly, since cone spacing and density measures represent light reflected by photoreceptors in which the photoreceptor interface with the RPE and the inner segment/outer segment junction is intact,²⁷ photoreceptor nuclei may persist in regions where the outer and inner segments have degenerated, explaining the difference observed in cone density from AOSLO images despite similar ONL thicknesses. Alternatively, the ONL thickness may be increased in eyes with RP compared to healthy eyes as a consequence of retinal remodeling which occurs during retinal degeneration.^{28,29} Retinal remodeling encompasses different phases, initially manifest as altered synaptic connections and neurite sprouting of stressed photoreceptors; subsequent photoreceptor death, cell body phagocytosis, and Müller cell hypertrophy, and eventual migration of the surviving neurons and glial cells.²⁹ Chui et al.⁶ found that cone density measures decrease while ONL thickness increases with age, possibly also a consequence of retinal remodeling processes. Retinal remodeling processes might lead to thickening of retinal layers despite photoreceptor degeneration.^{29,30} Including additional RP patients with more advanced disease in future studies may demonstrate significant changes in ONL thickness with more pronounced photoreceptor loss.

In the present study, there were more females than males in the RP group (58%) compared to the normal subjects (30%). According to Wagner-Schuman et al.³¹ women have thinner central retinal thicknesses than men. In the present study, CRT was significantly thinner among female than male normal subjects ($P = 0.009$), but in the patient group female CRT values were thicker than males, perhaps due to variations in

disease severity or retinal remodeling. These findings are further evidence of the complexity of the structural changes occurring in retinal degeneration and could explain why cone densities were lower in patients with RP but ONL thicknesses were similar to normal eyes.

In conclusion, ONL thickness and cone density were significantly correlated in normal subjects and patients with RP. The correlation was weaker between 1.5° and 3° from the fovea than 0.5° and 1.5° from the fovea for normal subjects and patients with RP, likely due to the increasing number of rod photoreceptors contributing to the ONL thickness with increasing eccentricity from the fovea. However, the relationship between ONL thickness and cone density likely is strongly dependent on the relationship between both these variables and retinal eccentricity. We observed a range of cone density values around the best-fit regression line, making it challenging to predict cone density from ONL thickness, even when ONL thickness was measured with exclusion of HFL from D-OCT scans. Cone density was lower in RP patients with excellent visual acuity, while the ONL thickness in the central retina was comparable to normal subjects, suggesting that cone density derived from AOSLO images may provide a more sensitive measure of disease progression in RP than ONL thickness measures even when the HFL is excluded using D-OCT.

Acknowledgments

The authors thank Radha Ayyagari, PhD, for whole exome sequencing to identify the mutation in patient 40032.

Supported by NIH Grants EY002162 (JLD), EY014375 (AR), R01EY017607 and P30EY001931 (JC), and EY017269 (BJL), and the Foundation Fighting Blindness (JLD), a Physician Scientist Award, and unrestricted funds from Research to Prevent Blindness (JLD), That Man May See, Inc. (JLD, TCP), Hope for Vision (JLD), and the George and Rosalie Hearst Foundation (MM).

Disclosure: **M. Menghini**, None; **B.J. Lujan**, None; **S. Zayit-Soudry**, None; **R. Syed**, None; **T.C. Porco**, None; **K. Bayabo**, None; **J. Carroll**, None; **A. Roorda**, None; **J.L. Duncan**, None

References

- Jacobson SG, Roman AJ, Aleman TS, et al. Normal central retinal function and structure preserved in retinitis pigmentosa. *Invest Ophthalmol Vis Sci*. 2010;51:1079-1085.
- Wang R, Jiang C, Ma J, Young MJ. Monitoring morphological changes in the retina of *rhodopsin*^{-/-} mice with spectral domain optical coherence tomography. *Invest Ophthalmol Vis Sci*. 2012;53:3967-3972.
- Pennesi ME, Michaels KV, Magee SS, et al. Long-term characterization of retinal degeneration in *rd1* and *rd10* mice using spectral domain optical coherence tomography. *Invest Ophthalmol Vis Sci*. 2012;53:4644-4656.
- Aleman TS, Cideciyan AV, Sumaroka A, et al. Retinal laminar architecture in human retinitis pigmentosa caused by *Rhodopsin* gene mutations. *Invest Ophthalmol Vis Sci*. 2008;49:1580-1590.
- Curcio CA, Sloan KR, Kalina RE, Hendrickson AE. Human photoreceptor topography. *J Comp Neurol*. 1990;292:497-523.
- Chui TY, Song H, Clark CA, Papay JA, Burns SA, Elsner AE. Cone photoreceptor packing density and the outer nuclear layer thickness in healthy subjects. *Invest Ophthalmol Vis Sci*. 2012;53:3545-3553.
- Curcio CA, Messinger JD, Sloan KR, Mitra A, McGwin G, Spaide RF. Human chorioretinal layer thicknesses measured in macula-wide, high-resolution histologic sections. *Invest Ophthalmol Vis Sci*. 2011;52:3943-3954.
- Curcio CA, Millican CL, Allen KA, Kalina RE. Aging of the human photoreceptor mosaic: evidence for selective vulnerability of rods in central retina. *Invest Ophthalmol Vis Sci*. 1993;34:3278-3296.
- Lujan BJ, Roorda A, Knighton RW, Carroll J. Revealing Henle's fiber layer using spectral domain optical coherence tomography. *Invest Ophthalmol Vis Sci*. 2011;52:1486-1492.
- Talcott KE, Ratnam K, Sundquist SM, et al. Longitudinal study of cone photoreceptors during retinal degeneration and in response to ciliary neurotrophic factor treatment. *Invest Ophthalmol Vis Sci*. 2011;52:2219-2226.
- Duncan JL, Roorda A, Navani M, et al. Identification of a novel mutation in the *CDHR1* gene in a family with recessive retinal degeneration. *Arch Ophthalmol*. 2012;130:1301-1308.
- Makhijani VS, Roorda A, Bayabo JK, Tong KK, Rivera-Carpio CA, Lujan B. Chromatic visualization of reflectivity variance within hybridized directional OCT images. Paper presented at: *Proc SPIE8571, Optical Coherence Tomography and Coherence Domain Optical Methods in Biomedicine XVII*, 857105; February 2, 2013; San Francisco, CA. <http://proceedings.spiedigitallibrary.org/proceeding.aspx?articleid=1670789>.
- Duncan JL, Zhang Y, Gandhi J, et al. High-resolution imaging with adaptive optics in patients with inherited retinal degeneration. *Invest Ophthalmol Vis Sci*. 2007;48:3283-3291.
- Lindeman RH, Merenda PF, Gold RZ. *Introduction to Bivariate and Multivariate Analysis*. Glenview, IL: Scott, Foresman; 1980.
- Tick S, Rossant F, Ghorbel I, et al. Foveal shape and structure in a normal population. *Invest Ophthalmol Vis Sci*. 2011;52:5105-5110.
- Ooto S, Hangai M, Tomidokoro A, et al. Effects of age, sex, and axial length on the three-dimensional profile of normal macular layer structures. *Invest Ophthalmol Vis Sci*. 2011;52:8769-8779.
- Drexler W, Sattmann H, Hermann B, et al. Enhanced visualization of macular pathology with the use of ultrahigh-resolution optical coherence tomography. *Arch Ophthalmol*. 2003;121:695-706.
- Anger EM, Unterhuber A, Hermann B, et al. Ultrahigh resolution optical coherence tomography of the monkey fovea. Identification of retinal sublayers by correlation with semithin histology sections. *Exp Eye Res*. 2004;78:1117-1125.
- Zawadzki RJ, Jones SM, Olivier SS, et al. Adaptive-optics optical coherence tomography for high-resolution and high-speed 3D retinal in vivo imaging. *Opt Express*. 2005;13:8532-8546.
- Roorda A, Romero-Borja F, Donnelly W III, Queener H, Hebert T, Campbell M. Adaptive optics scanning laser ophthalmoscopy. *Opt Express*. 2002;10:405-412.
- Chui TY, Song H, Burns SA. Adaptive-optics imaging of human cone photoreceptor distribution. *J Opt Soc Am A Opt Image Sci Vis*. 2008;25:3021-3029.
- Duncan JL, Talcott KE, Ratnam K, et al. Cone structure in retinal degeneration associated with mutations in the *peripherin/RDS* gene. *Invest Ophthalmol Vis Sci*. 2011;52:1557-1566.
- Carroll J. Adaptive optics retinal imaging: applications for studying retinal degeneration. *Arch Ophthalmol*. 2008;126:857-858.
- Li KY, Tiruveedhula P, Roorda A. Intersubject variability of foveal cone photoreceptor density in relation to eye length. *Invest Ophthalmol Vis Sci*. 2010;51:6858-6867.
- Hood DC, Lazow MA, Locke KG, Greenstein VC, Birch DG. The transition zone between healthy and diseased retina in patients with retinitis pigmentosa. *Invest Ophthalmol Vis Sci*. 2011;52:101-108.

26. Milam AH, Li ZY, Fariss RN. Histopathology of the human retina in retinitis pigmentosa. *Prog Retin Eye Res.* 1998;17:175-205.
27. Putnam NM, Hammer DX, Zhang Y, Merino D, Roorda A. Modeling the foveal cone mosaic imaged with adaptive optics scanning laser ophthalmoscopy. *Opt Express.* 2010;18:24902-24916.
28. Jacobson SG, Cideciyan AV, Sumaroka A, et al. Remodeling of the human retina in choroideremia: rab escort protein 1 (*REP-1*) mutations. *Invest Ophthalmol Vis Sci.* 2006;47:4113-4120.
29. Jones BW, Watt CB, Frederick JM, et al. Retinal remodeling triggered by photoreceptor degenerations. *J Comp Neurol.* 2003;464:1-16.
30. Li ZY, Kljavin IJ, Milam AH. Rod photoreceptor neurite sprouting in retinitis pigmentosa. *J Neurosci.* 1995;15:5429-5438.
31. Wagner-Schuman M, Dubis AM, Nordgren RN, et al. Race- and sex-related differences in retinal thickness and foveal pit morphology. *Invest Ophthalmol Vis Sci.* 2011;52:625-634.